Microporous and Mesoporous Materials 118 (2009) 202–209

Contents lists available at ScienceDirect

Microporous and Mesoporous Materials

journal homepage: www.elsevier.com/locate/micromeso

Microporous niobia–silica membranes: Influence of sol composition and structure on gas transport properties

V. Boffa [1], J.E. ten Elshof *, R. Garcia, D.H.A. Blank

Inorganic Materials Science, MESA + Institute for Nanotechnology and Faculty of Science and Technology, University of Twente, P.O. Box 217, 7500 AE Enschede, The Netherlands

ARTICLE INFO

Article history:
Received 24 May 2008
Received in revised form 30 July 2008
Accepted 17 August 2008
Available online 28 August 2008

Keywords:
Sol–gel
Separation
Hydrogen
Carbon dioxide
XPS

ABSTRACT

Three different microporous niobia–silica gas separation membranes with an exceptionally low permeability for CO_2 were prepared and their permeabilities for different gases were compared. The Nb:Si molar ratios of the sols varied between 0.33 and 0.8, and the radii of gyration varied between 2.4 and 3.2 nm, respectively. All three sols showed narrow particle size distributions, and no particles with hydrodynamic diameters above 60 nm were detected. The hydrogen and helium permeabilities of membranes could be correlated with the degree of structural evolution of the sols. The structurally least developed sol yielded more resistive membrane films. The increase in the loading of Nb^{5+} ions in the silica framework led to an increase of the H_2/CO_2 separation factor from ~40 to 70, but also caused densification of the material, leading to a much more resistive network. Single gas permeation measurements showed a preferential permeability towards helium at 200 °C for all the membranes. X-ray photoelectron spectroscopy analysis of a niobia–silica thin film showed that it had a homogeneous distribution of Si and Nb atoms, and that this material exhibited a different interaction with CO_2 than pure silica and pure niobia surfaces do.

1. Introduction

Recently we reported the preparation of a niobia–silica (NS) microporous membrane from a sol with a Nb:Si molar ratio equal to 0.33 [1]. Because of its very low permeability for CO_2 compared to other gas molecules, e.g. He, H_2, O_2 and CH_4, such NS-type membranes may be of interest for industrial separation processes in which CO_2 is involved. The selectivity of the membrane is thought to be based on a combination of size-based sieving and variations in molecule-wall interactions between different types of gases. The presence of pentavalent niobium ions in the microporous silicon oxide matrix probably introduces active surface sites in the thin film to which carbon dioxide binds [1,2]. Niobia–silica membranes also have a higher hydrothermal stability than microporous silica membranes [3]. NS membranes might therefore find application in large-scale industrial processes like steam reforming and water gas shift reaction. However, the development of NS membranes is still in a premature stage and the hydrogen permeability of NS films is still about one order of magnitude smaller than what can be achieved with silica membranes [3]. For this reason, the processing conditions of NS–type membranes need further optimization.

A large number of parameters play a role in the fabrication of a membrane, e.g. sol concentration and viscosity, deposition rate, type of support, calcination temperature, calcination time and heating/cooling rates of the furnace. Moreover, a membrane can be aged under certain conditions to control the evaporation rate of the solvent during consolidation prior to calcination [4–7]. Because of the complexity of the process, it is not yet possible to construct a general model that can predict the main membrane properties (porosity, pore size distribution, and layer thickness) from the processing procedure. The development of ceramic membranes is therefore still done via experimental approaches [8].

In the present report, we selected three recipes, hereinafter designated as NS1, NS2 and NS3, to study the influence of sol type and composition on membrane properties. The preparation and characterization of the NS1 sol and of the resulting NS1 membrane have been already reported [1]. The NS2 sol was prepared from the same reaction mixture as the NS1 sol, but it was refluxed for 90 min instead of 300 min at 60 °C, and thus it had smaller particles than NS1. The NS3 sol was synthesized from a precursor mixture with a higher Nb:Si atomic ratio than NS1 and NS2, but the particle size was comparable with that of NS1. Disk membranes were processed from these sols and characterized, and their properties were compared. As will be shown in this study, the permselectivity and permeability can be correlated with the characteristics of the sol from which the films were generated. These experiments aim to establish an understanding of the relationship between sol structure and membrane properties.

* Corresponding author. Tel.: +31 53 489 2695; fax: +31 53 489 3595.
E-mail address: j.e.tenelshof@utwente.nl (J.E. ten Elshof).
[1] Present address: Dipartimento di Chimica Generale e Chimica Organica, Università di Torino, Corso M. D'Azeglio 48, 10125 Torino, Italy.

1387-1811/$ - see front matter © 2008 Elsevier Inc. All rights reserved.
doi:10.1016/j.micromeso.2008.08.038

2. Experimental part

2.1. Synthesis of niobia–silica sols

Eleven millilitre of tetraethyl orthosilicate (Aldrich, 99.999% pure) was added to 10.5 ml of ethanol. A mixture of 0.14 ml of HNO_3 (65%, Fluka) in 1.8 ml of water was dropped into the mixture. The final molar ratio (Si)–O–C_2H_5:H_2O:HNO_3 was 1:0.5:0.01. We chose to express the chemical composition of the sol in this way because alkoxy groups, water and acid are the moieties that participate directly in the reaction. This mixture was heated under reflux at 60 °C for 2 h. Then 6.62 ml of 1 M niobium(V)penta(*n*-butoxide) (Gelest) in *n*-butanol (Aldrich, anhydrous) was added slowly to the mixture. Aqueous nitric acid was dropped into the mixture to restore the initial composition (M)–O–R:H_2O:HNO_3 to 1:0.5:0.01, with M = Si, Nb and R = $-C_2H_5$ or $-C_4H_9$. The Nb:Si atomic ratio in the sol was 0.33. Thereafter the NS1 sol was refluxed at 60 °C for 300 min. For the NS2 sol the same procedure was used as for the NS1 sol, except that the final reflux took 90 min instead of 300 min.

The preparation of the NS3 sol consisted of dropwise adding aqueous nitric acid (0.833 ml HNO_3 65% in 3.9 ml of water) to a mixture of 13 ml of TEOS and 136 ml of ethanol. The mixture was refluxed for 2 h at 60 °C. After this time, an aliquot of 16.5 ml of this sol was mixed to 5 ml of a 1 M solution of niobium(V) penta(*n*-butoxide) in *n*-butanol. The mixture was heated to 60 °C for 90 min. The final molar ratio (M)–O–R:H_2O:HNO_3 in NS3 was 1:0.5:0.025 and the Nb:Si molar ratio was 0.8.

2.2. Characterization of niobia–silica sols

SAXS measurements were performed at the BM-26B station of the Dutch–Belgian beam line (DUBBLE) [9] at the European synchrotron radiation facility (ESRF) in Grenoble, France. The samples were placed in capillary glass tubes (Ø 1.5 mm, glass no. 14, Hildenberg, Malsfeld, Germany). In order to cover the largest possible *q*-range, measurements were performed twice on all capillaries, namely with the 2D CCD detector located at 1.5 m and at 8 m away from the sample, respectively. The tubes were exposed to a 12 keV X-ray beam, which corresponds to a wavelength of 0.13 nm.

Dynamic light scattering (DLS) measurements were performed on a Malvern Zetasizer HS3000. The correlograms were analyzed by using the CONTIN method [10].

2.3. Powder preparation and analysis

Aliquots of the sols were dried in Petri-dishes in air and calcined at 500 °C for 3 h, with a heating/cooling rate of 0.5 °C/min. These conditions are similar to the preparation conditions used for making membranes. The presence of crystalline phases in these powders was determined by XRD analysis using a Philips SR5056 with Cu Kα radiation.

2.4. XPS analysis of thin films on silicon substrates

Three silicon wafers were etched to remove the native silicon oxide surface layer and then were coated by sputtering with a 5 nm thick gold layer. The NS1 sol, a 1 M solution of TEOS in ethanol and a 1 M solution of niobium(V) penta (*n*-butoxide) in *n*-butanol were spin-coated at 2000 rpm for 60 s. The samples were calcined at 500 °C to yield three oxide films. After cooling the samples were immersed in a dry CO_2 bath for 12 h and then heated again at 200 °C to simulate the membrane life cycle. X-ray photoelectron spectroscopy (XPS) measurements were performed on a PHI Quantera Scanning ESCA Microprobe equipped with a monochromatic Al Kα X-ray source (1486.6 eV) at a pressure $<2 \times 10^{-6}$ bar. To remove any unknown contaminants, a layer with a thickness of about 0.5 nm was removed by etching with Ar^+ before analysis. The data reported here represent average values of three points that were selected on each sample.

2.5. Membrane coating

α-Alumina disks (2 mm thick, Ø 39 mm), fabricated as described elsewhere [7], were used as supports. These supports were polished on one side and coated with a 6% La-doped γ-alumina film of about 2 μm thickness [1], dried and calcined at 600 °C. After dilution of the niobia–silica sols, they were deposited by dip coating in a class 1000 clean room. The extent of dilution is reported in Table 1 for each sol. The membranes were calcined in air at 500 °C for 3 h, with heating and cooling rates of 0.5 °C/min.

2.6. Gas permeance measurements

The He, H_2, CO_2, N_2, CH_4 and SF_6 permeances of a disk-shaped γ-alumina support and of the microporous NS membranes coated on such supports were measured in a dead-end mode permeation set-up. Since atmospheric water can condense in micropores at these temperatures, all membranes were dried in a hydrogen flow for at least 16 h after the temperature had been raised to 200 °C. The gas flow rate was measured with a soap film flow meter, while the overpressure across the membrane was kept constant at 4 bar. The permeation rates of the different gases were determined in a sequence starting with the one with the smallest kinetic diameter, from helium to SF_6. For each probe molecule the temperature of the furnace was varied step-wise from 200° C down to 80 °C. The calculated error in the permeation measurements was about 2% for permeances above 10^{-9} mol Pa^{-1} m^{-2} s^{-1}, and less than 6% for permeances below 10^{-9} mol Pa^{-1} m^{-2} s^{-1}.

Table 1
Characteristics of the sols used for the preparation of membranes

Membrane	Nb:Si[a]	D_f [b]	R_g [nm][c]	R_H [nm][d]			Polydispersity		Sol concentration (v/v)[e]
				$\langle R_H\rangle_I$	$\langle R_H\rangle_V$	$\langle R_H\rangle_N$	$\langle R_H\rangle_I/\langle R_H\rangle_N$	$\langle R_H\rangle_V/\langle R_H\rangle_N$	
NS1	0.33	1.8	3.2 ± 0.1	7.6	2.5	1.7	4.4	1.5	9%
NS2	0.33	1.7	2.4 ± 0.1	5.3	2.0	1.4	4.0	1.5	2%
NS3	0.80	1.8	3.5 ± 0.1	9.6	2.8	1.8	5.5	1.6	2%

[a] Molar ratio of the metal alkoxide precursors.
[b] Fractal dimension as obtained from SAXS.
[c] Gyration radius as obtained from SAXS.
[d] Hydrodynamic radius as obtained from DLS (average in number). $\langle R_H\rangle_I$ = average on scattered intensity, $\langle R_H\rangle_V$ = average on particle volume, $\langle R_H\rangle_N$ = average on particle number.
[e] Dilution in ethanol before coating, expressed in terms of volume of sol/volume of final coating solution.

3. Results and discussion

3.1. Characterization of NS sols

Table 1 provides information about the coating sols that were used for membrane preparation and about the sol particles properties as measured by SAXS and DLS. In SAXS the scattered light intensity of a incoming beam is measured as a function of scattering angle. This allows determination of the gyration radius (R_g) of a particle with a mass M, and the fractal dimension (D_f), which is defined by Eq. (1) [11,12].

$$M \propto R_g^{D_f} \quad (1)$$

All sols turned out to have fractal dimensions of 1.7–1.8, but their effective sizes in solution are considerably different. From the SAXS measurements it was concluded that the NS1 sol was composed of particles with a main gyration radius (R_g) of 3.2 ± 0.1 nm. The NS2 and NS3 sols had an R_g of 2.4 ± 0.1 nm and 3.5 ± 0.1 nm, respectively. Because the gyration radius is only a mean value, the three samples were also analyzed by DLS to determine their particle size distributions. Fig. 1 shows the results of this analysis. Three distributions are given for each sample: scattered intensity, particle volume and particle number, each as a function of the hydrodynamic radius (R_H), which is the radius of a hard sphere having the same diffusion coefficient as the sol particles.

The average hydrodynamic radii calculated from these three distributions are $\langle R_H\rangle_I$, $\langle R_H\rangle_V$ and $\langle R_H\rangle_N$, which values refer to the average of intensity, volume and number distributions, respectively. The average radii calculated for each sample are reported in Table 1. A $\langle R_H\rangle_N$ of 1.7 nm was measured for NS1, while these values were 1.4 nm for NS2 and 1.8 nm for NS3, respectively. They are smaller than the R_g values measured by SAXS, however they reflect the same trend: NS1, NS3 > NS2.

For a completely monodisperse sample the values of $\langle R_H\rangle_I$, $\langle R_H\rangle_V$ and $\langle R_H\rangle_N$ should coincide. In polydisperse samples they all have different values. The averages increase in the order $\langle R_H\rangle_N < \langle R_H\rangle_V < \langle R_H\rangle_I$, because the scattered intensity is proportional to the sixth power of the radius of scattering particles, $I \propto R_H^6$ [13], and the volume distribution was calculated by assuming spherical particles, i.e. $V \propto R_H^3$. Essentially, the ratios $\langle R_H\rangle_V/\langle R_H\rangle_N$ and $\langle R_H\rangle_I/\langle R_H\rangle_N$ are qualitatively similar to the molecular mass ratios M_W/M_N and M_Z/M_N, which define the polydispersity indexes of polymeric mass distributions [14]. In the latter expressions M_N, M_W and M_Z represent the number, weight and z average molecular mass of a polymer.

The polydispersity indexes are listed in Table 1. The ratio $\langle R_H\rangle_V/\langle R_H\rangle_N$ is similar for all three samples and ranges between 1.5 and 1.6. The polydispersity index $\langle R_H\rangle_I/\langle R_H\rangle_N$ instead, revealed differences between the polydispersities of the samples. NS2 and NS1 were prepared from mixtures having the same molar composition but reacted for different times, i.e., 90 and 300 min, respectively. During the extra 210 min in which NS1 was allowed to develop further, the sol particles grew and the polydispersity index $\langle R_H\rangle_I/\langle R_H\rangle_N$ increased from 4.0 to 4.5. The increase can simply be attributed to the statistical broadening that occurs during the progress of the polymerization reaction [15, 16].

The NS3 sol, which was based on the highest concentration of Nb precursor, appeared to have a broader size distribution than the two other samples, although it was refluxed for only 90 min. This suggests that the niobium precursor, which is more reactive and has more functional groups than TEOS, has a tendency to yield more polydisperse particle size distributions.

The DLS data also revealed that none of the sols contained particles with a hydrodynamic radius larger that 60 nm. The niobia–silica sols presented in this study are therefore potentially suitable precursors for making microporous thin layers.

3.2. XRD analysis of powders

The three powders were analyzed by XRD to check the presence of crystallinity in the samples. All samples appeared to be non-crystalline. The absence of XRD peaks in all samples indicates that the niobium atoms were either atomically dispersed in the silica matrix, or had crystallite sizes smaller than 2–3 nm, which is the detection limit for Cu-Kα radiation [17,18]. These results agree well with the data reported by Francisco et al. for sol–gel derived niobium-doped silica powders with ⩽7.5% Nb [19]. A crystalline niobium-containing phase was observed only in samples that had been annealed above 800 °C.

3.3. Permeabilites of the microporous materials

After coating and calcination, selective separation layers with different thicknesses were obtained, as illustrated in Fig. 2. The niobia–silica top layer of the NS1 membrane was 150 nm thick [1], while the NS2 and NS3 films had thicknesses of 60 and 100 nm, respectively.

Table 2 reports the hydrogen and helium permeances F of the three membranes. In the case of NS2, the helium permeance was 1.2×10^{-8} mol Pa^{-1} m^{-2} s^{-1} and the hydrogen permeance was 4.5×10^{-9} mol Pa^{-1} m^{-2} s^{-1}. The NS3 membrane had a higher permeance for helium, but a lower permeance for hydrogen.

The permeability of the top layer material is defined as the permeance per unit of membrane thickness. To calculate the permeability of the NS layers it is necessary to extract the top layer permeance from the overall permeance of the membrane. Since

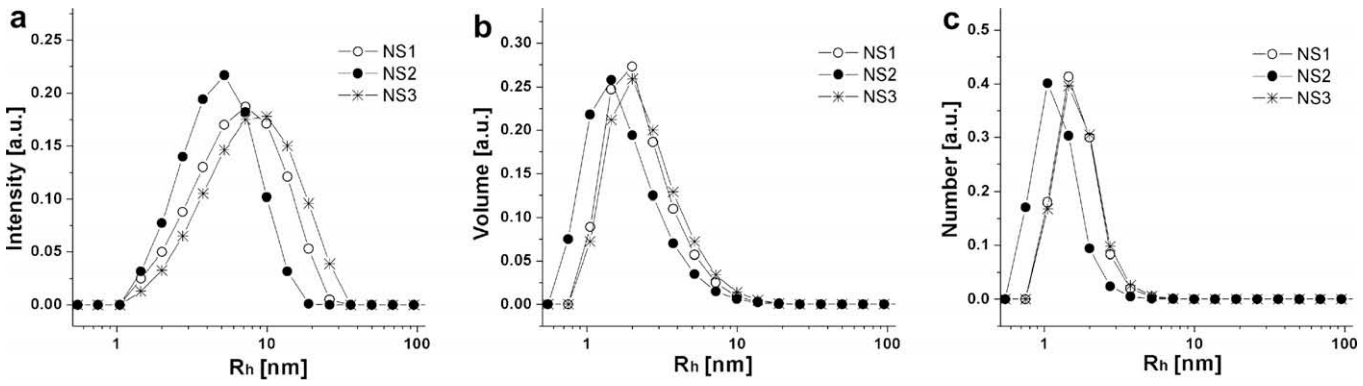

Fig. 1. Particle size distribution of NS1, NS2 and NS3 sols obtained by DLS. The graphs represent the (a) intensity, (b) volume and (c) number distributions. The areas under the curves were normalized to unity.

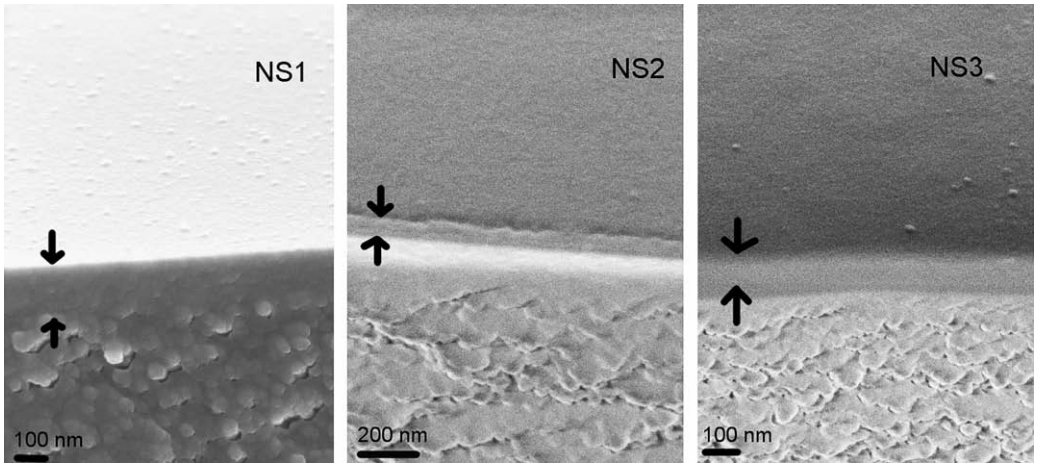

Fig. 2. SEM images of cross-sections of the NS membranes. The locations of the top layers are indicated by arrows.

Table 2
Permeance, permeability and ideal permselectivity of NS membranes

	Permeance[a] [mol Pa^{-1} m^{-2} s^{-1}]		Ideal selectivity		Top layer thickness [nm]	Permeability[b] [mol Pa^{-1} m-1 s^{-1}]	
	He	H_2	He/H_2	He/CO_2		He	H_2
NS1	7.2×10^{-8}	3.8×10^{-8}	1.9	43	150	1.2×10^{-14}	5.7×10^{-15}
NS2	1.2×10^{-8}	4.5×10^{-9}	2.7	37	60	7.3×10^{-16}	2.7×10^{-16}
NS3	2.8×10^{-8}	3.7×10^{-9}	7.6	70	100	2.9×10^{-15}	3.7×10^{-16}

Data refer to measurements conducted at 200 °C, ΔP = 4 bar
[a] Permeance of the entire stacked membrane.
[b] Permeability is permeance multiplied by top layer thickness.

the membrane is a stack of layers, the total resistance of the membrane is the sum of resistances of each layer. The transport resistance is proportional to the inverse of permeance. The permeance of the NS–layers can thus be determined from the total permeance and the permeance of the support via [20]:

$$\frac{1}{F_{tot}} = \frac{1}{F_{NS}} + \frac{1}{F_{Sup}}, \quad (2)$$

where $1/F_{tot}$ is the total resistance, and $1/F_{NS}$ and $1/F_{Sup}$ are the resistances of top layer and support, respectively.

In order to determine the support resistance, the permeance of the α-alumina supported γ-alumina support was measured at different temperatures for the different probes. The results are shown in Fig. 3. The data were fitted following a Knudsen-type permeation model [21]:

$$F_{sup} = K\sqrt{\frac{1}{MRT}}, \quad (3)$$

where K is a constant that depends only on geometrical membrane properties (i.e., thickness, porosity, pore size and shape), M is the molecular mass of the permeating molecule, R is the gas constant and T is the absolute temperature. Fig. 3 shows that the transport rate in the support shows Knudsen-type behaviour, as is typical for mesoporous system such as γ-alumina. The constant K was determined to have a value of $8.9 \times 10^{-5} \pm 1 \times 10^{-6}$ kg Pa^{-1} m^{-1} s^{-2} by linear fitting Eq. (3) to the data points of Fig. 3 (correlation coefficient 0.998). This indicates that the contribution of viscous flow is almost irrelevant to the total transport in the support [22]. Following this method it was possible to determine the support resistance at different temperatures and for different probes.

The H_2, He and CO_2 permeances of the individual niobia–silica layers were calculated using Eq. (2). The permeabilities of the niobia–silica layers for helium and hydrogen are listed in Table 2. The

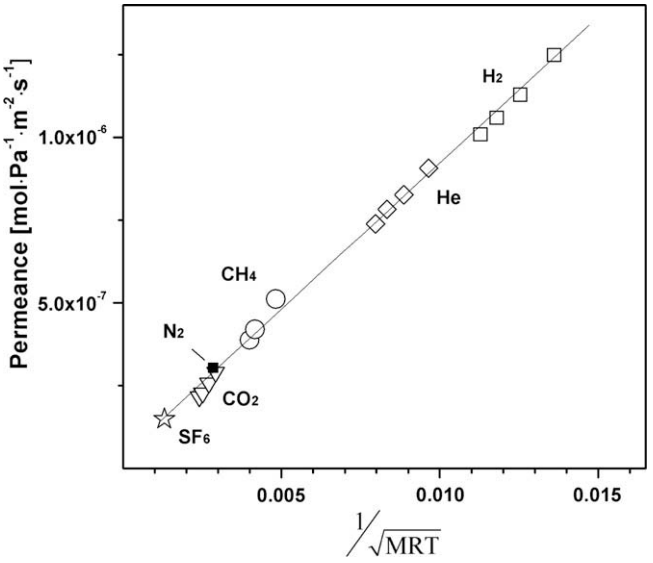

Fig. 3. Permeance of 6 probe molecules through a α-alumina supported γ-alumina disk of the same type used as support for the microporous top layers presented here. The straight line represents the linear fit of the data to Eq. (3).

material forming the NS1 top layer is more permeable to these small gas molecules than NS2 and NS3. Comparison of NS1 with NS2 shows that the hydrogen permeability decreased from 5.7×10^{-15} to 2.7×10^{-16} mol Pa^{-1} m^{-1} s^{-1}, while the helium permeability decreased from 1.2×10^{-14} to 7.3×10^{-15} mol Pa^{-1} m^{-1} s^{-1}. The large difference in permeability is somehow related to the evolution of the structure of the coating sols during synthesis. XPS analysis of the NS1 membrane reported previously [1] suggests that unreacted TEOS molecules or silica oligomers were still

present even in the NS1 sol. When such small particles or pre-polymeric structures become trapped in the top layer during film formation, a relatively dense material will result after consolidation and calcination. Since the NS2 sol was less developed than NS1, it is reasonable to assume that the concentration of unreacted species was particularly high in NS2. Consequently, the resistivity of this layer after calcination was higher than that of the NS1 layer.

Fig. 1 shows that NS2 contains a large number of particles with R_H smaller than 1 nm. Thus, they may easily penetrate into the pores of the underlying γ-alumina layer with its 5–8 nm pore diameter [7]. The SEM picture in Fig. 2 shows that the NS2 sol indeed penetrated into the support down to a depth of about 50 nm or more. Because of this, the thickness of the NS2 top layer may be underestimated, as well as its permeability.

By comparing the particle size distribution, $\langle R_H \rangle_I$ and R_g of sols NS1 and NS3, it appears that NS3 was developed further than NS1, even though it had reacted for a shorter time. Thus, the reason for the low H_2 and He permeances of the NS2 membrane does not hold for NS3. Although the particle size of NS3 is similar to that of NS1, its Nb:Si molar ratio is considerably higher. The Nb_{5+} ions in the network have a coordination number equal to 6 [23], while Si_{4+} has a coordination number of 4 [24]. The presence of the more highly charged Nb ions, and the ability and tendency of Nb to coordinate more oxygen ions may lead to a more closely packed and denser network. The effect is most pronounced in NS3, since the concentration of Nb ions is higher than in the other samples. This may provide an explanation for the higher resistance of the NS3 layer.

The higher concentration of Nb in NS3 also affects separation. The ideal separation factor is defined as the ratio of single gas permeances of two gases. The ideal separation factor for He and H_2 is 7.6 for the NS3 membrane, as listed in Table 2. The corresponding ideal separation factors for NS1 and NS2 were 1.9 and 2.7, respectively. The separation factor He/CO_2 is also higher for the NS3 membrane than for the other two materials. In general, microporous membranes are more permeable to helium than to other gases, because helium is very small and hardly interacts with the pore walls due to its noble character. However, this tendency seems to be more pronounced in the NS3 membrane than in the other two. This may possibly be attributed to a predominance of pores in the NS3 membrane that are accessible to helium only.

3.4. Activated transport trough the membranes

To understand the transport mechanism that governs the permeance in niobia–silica layers in more detail, we studied the temperature dependency of the permeance of various gases. Fig. 4 shows the permeance of the NS1 membrane for different probe molecules. The flux of helium and hydrogen across the membrane increased exponentially with increasing temperature, while the reverse trend was observed for CO_2. The temperature dependency of N_2, CH_4 and SF_6 was more complex.

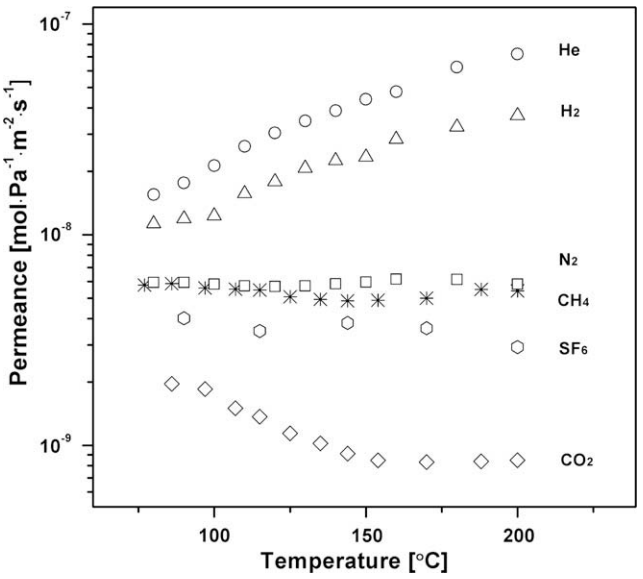

Fig. 4. Temperature dependency of permeance of several gases in the NS1 membrane. The plotted data refer to the permeances of the whole membrane thickness.

Gas transport in micropores occurs essentially according to a surface diffusion mechanism. The transport rate associated with this mechanism can be expressed in terms of a modified Fick law [20]:

$$J = J_0 \exp\left\{-\frac{E_a}{RT}\right\}\frac{\Delta P}{L}. \quad (4)$$

J_0 is a temperature independent coefficient and E_a is the apparent activation energy. E_a is the sum of two contributions: the heat of sorption of the molecule (here considered as a negative number, since adsorption is an exothermic process in which heat is released) and the positive activation energy of mobility of the permeating molecule inside the membrane matrix. Since these two terms have opposite signs the apparent activation energy can be positive or

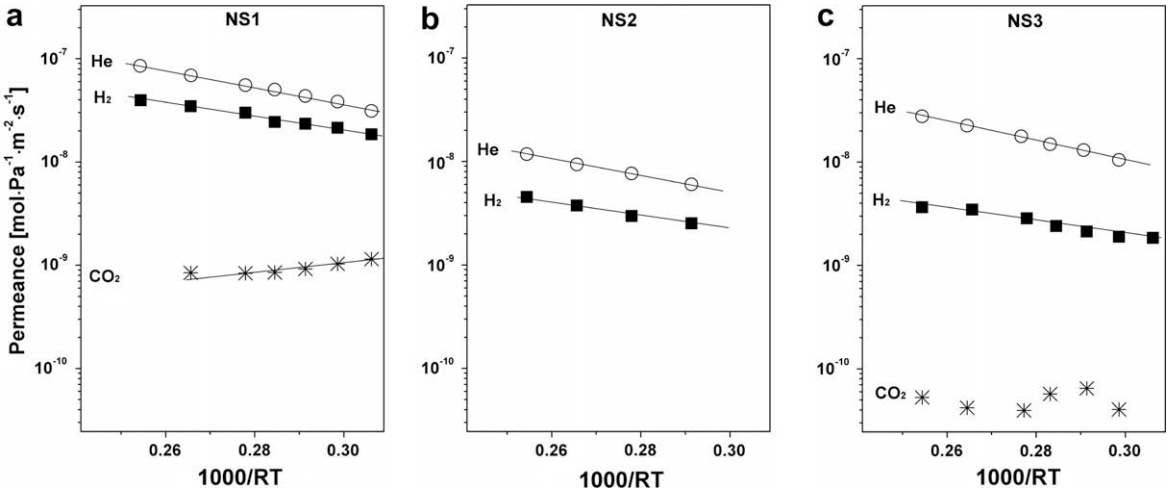

Fig. 5. Temperature dependency of He, H_2 and CO_2 permeance in top layers of NS1, NS2 and NS3.

negative depending on their relative magnitudes. A negative value of E_a is generally interpreted as being caused by strong adsorption of the molecule on the pore surface. The change of slope in the CO_2 permeance above 150 °C may be due to a change of the predominant transport mechanism, and these data were not included in the activation energy calculations discussed below.

The temperature dependencies of the He, H_2 and CO_2 permeances in all three top layers are shown in Fig. 5. The corresponding apparent activation energies are listed in Table 3. The apparent activation energy of hydrogen permeance is similar for all three samples, and is about 15–16 kJ mol^{-1}. The activation energy of He permeance in the NS3 membrane is 22.0 ± 0.9 kJ mol^{-1}, and has a slightly lower value in the other two materials (18–19 kJ mol^{-1}). These differences are in agreement with the single gas permeation data of Table 2, which showed a preferential permeability towards helium at 200 °C, especially for the NS3 sample. Due to experimental limitations in measuring permeances below 10^{-10} mol Pa^{-1} m^{-2} s^{-1}, the apparent activation energy of the CO_2 permeance in NS2 and NS3 could not be determined. Its value is equal to −14.8 ± 0.8 kJ mol^{-1} for NS1. Such a negative value is probably caused to a high enthalpy of sorption of the CO_2 molecules on the walls of the niobia–silica micropores, and has never been reported for pure silica [20,25–30]. Hence, the strong heat of adsorption should be related to the presence of Nb ions in the microporous framework [1].

Table 3
Apparent activation energies of H_2, He and CO_2 permeance in Nb-doped silica membranes, as calculated by fitting the data in Fig. 5 to Eq. (4)

	He apparent E_a [kJ mol^{-1}]	H_2 apparent E_a [kJ mol^{-1}]	CO_2 apparent E_a [kJ mol^{-1}]
NS1	19.1 ± 0.3	15.3 ± 0.7	−14.2 ± 0.8
NS2	18.1 ± 1.2	16.3 ± 1.0	–
NS3	22.0 ± 0.9	15.0 ± 1.2	–

3.5. XPS study of NS1 film

We studied the surface composition of the NS1 film by XPS to investigate the extent to which silicon and niobium atoms are mixed in the oxide matrix, and to establish a further understanding of the unusually strong interaction between CO_2 and the niobia–silica matrix [1]. The results were compared with XPS analyses of pure silica and niobia films.

All three XPS samples were exposed to CO_2 prior to analysis by immersing them in a dry CO_2 bath for 12 h. Before introducing the samples in the high vacuum system of the instrument, they were heated to 200 °C for 16 h to simulate the pretreatment of the

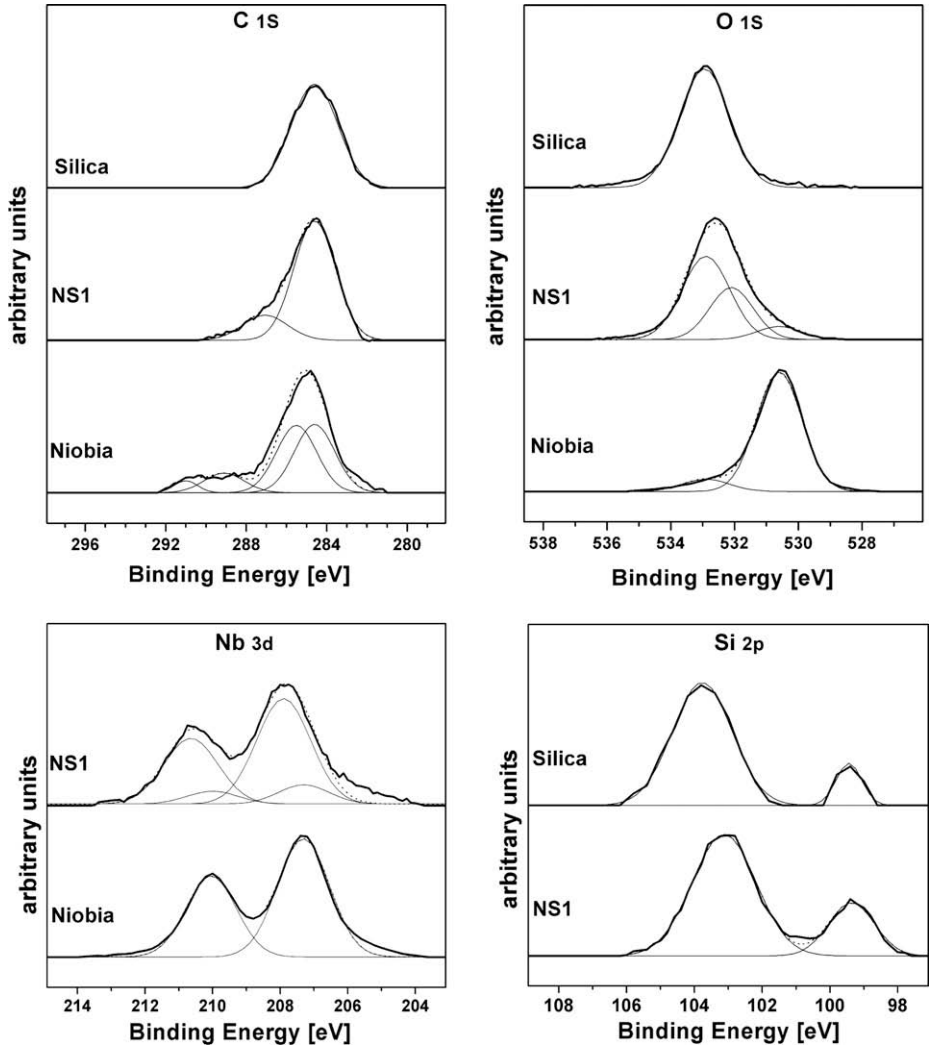

Fig. 6. XPS analysis of NS1 film on a Si wafer, and two reference films composed of silica and niobia, respectively. Bold lines represent experimental data after baseline subtraction; the thin lines indicate the fits based on Gaussian functions; the dotted line represents the sum of the single peak fits.

niobia–silica membranes. Fig. 6 and Table 4 show the resulting C 1s, O 1s, Nb 3d and Si 2p spectra of the three samples. We focused our analysis on the peak position, symmetry and full width at half maximum (FWHM).

The assignment of the C peak was done following the report of Cerruti et al. for glass samples [31]. The interaction of carbon dioxide with a metal oxide surface can be rather complex [32], as reflected in the spectra of NS1 and niobia. The C 1s peak at 284.6 eV (FWHM = 2.1 eV) is commonly assigned to graphitic and hydrocarbonaceous contaminants [33] and was used for calibration of the binding energy values. In the silica sample the peak was found to be completely symmetrical and no other carbon-containing species were detected. In contrast, the C 1s peak of NS1 was asymmetric and could be deconvoluted into two distinct signals centered at 284.6 eV (FWHM = 2.1 eV) and 287.1 eV (FWHM = 2.2 eV). The latter peak was assigned to surface carbonates and agrees with the IR signal at 1445 cm^{-1} observed by infrared spectroscopy on another NS1 film [1].

The deconvolution of the C 1s peak of the pure niobia sample was more complex and yielded a peak at 286.0 eV, and several other signals at a binding energy >288 eV. The latter peaks correspond to ionic carbonates (CO_3^{2-}) [31,32], which were probably formed during calcination or CO_2 exposure. The peak at 286.0 eV can be attributed to surface carbonates. The analysis of the C 1s peaks indicates that the NS1 sample is more reactive towards CO_2 than pure silica, and has a different reactivity than pure niobia since the binding energies of surface carbonates in the two samples were different. Because surface carbonates are still present in NS1 after treatment at 200 °C and degassing at a pressure $<2 \times 10^{-6}$ Pa, it is well possible that these species are strongly bonded to the NS1 surface and are not actively participating in CO_2 transport through the membrane. As already suggested [1], the low CO_2 permeance at 200 °C is probably determined by its interaction with surface cations, most likely with hydroxyl groups bonded to Nb ions. The fact that the surface carbonate and carbonate signals that were detected on pure niobia were not observed in the NS1 sample, can be taken as a further indication that niobia domains are absent in NS1.

Table 4
Assignment of XPS bands

Film	Binding energy (eV)	Peak width (FWHM) (eV)	Peak area (%)	Assignment
C 1s				
Silica	284.6	2.1	100	Adventitious C
NS1	284.6	2.1	81	Adventitious C
	287.1	2.2	19	surface carbonates
Niobia	284.6	2[a]	48	Adventitious C
	286.0	2[a]	36	surface carbonates
	289.1	2[a]	12	CO_3^{2-}
	291.0	1.3	4	CO_3^{2-}
O 1s				
Silica	532.9	1.6	100	Si–O–Si, Si–O–H
NS1	530.6[b]	1.5	5	Nb–O–Nb
	532.2	1.5	38	Nb–O–Si, Nb–O–H
	532.9[b]	1.2	57	Si–O–Si, Si–O–H
Niobia	530.4	1.4	91	Nb–O–Nb
	532.3	1.6	9	Nb–O–H
Si 2p				
Silica	99.4	1.4	42	Si^0 wafer
	103.1	1.9	58	SiO_4
NS1	99.4	0.8	15	Si^0 wafer
	103.8	2.0	85	SiO_4
Nb 3d				
NS1	207.3[c]	1.5[c]	9	$3d_{5/2}$ NbO_6
	207.9	1.6	52	$3d_{5/2}$ mixed ox.
	210.0[c]	1.5[c]	6	$3d_{3/2}$ NbO_6
	210.6	1.6	33	$3d_{3/2}$ mixed ox.
Niobia	207.3	1.5	60	$3d_{5/2}$ NbO_6
	210.0	1.5	40	$3d_{3/2}$ NbO_6

[a] Parameters arbitrarily chosen.
[b] Parameters fixed by adopting the O 1s binding energies from the pure silica and niobia films.
[c] Parameters fixed by adopting the Nb 3d binding energies from the niobia film.

The O 1s peak of the silica film could be fitted by a Gaussian centered at 532.9 eV (FWHM = 1.6 eV). The corresponding spectrum of pure niobia could be deconvoluted into two peaks. The main peak at 530.6 eV (FWHM = 1.4 eV) is commonly attributed to the bulk Nb_2O_5 [34] The shoulder at higher binding energies, in this case at 532.3 eV (FWHM = 1.6 eV), was also observed in niobium (V) oxide by Oliveira et al. [35], who assigned it to the hydroxyls groups on the niobia surface. The O 1s peak of the NS1 films is not symmetrical and has a maximum at 532.6 eV. In the niobium-silicon mixed oxide, oxygen may interact with Si, with Nb, with both Nb and Si, or belong to a surface hydroxyl group. The oxygen peak of NS1 were deconvoluted into three peaks with the restriction that two of the three peaks coincided with the binding energies and FWHM values of the pure niobia and silica peaks. The remaining third peak was centered at 532.2 eV (FWHM = 1.5 eV), which value is very close to the one that was attributed to Nb–O–H. The fact that its area was about 38% of the total signal area suggests that this peak also includes oxygen bonded to both Si and Nb centers. The area of this peak is about 7.6 times larger than that of the Nb–O–Nb peak, which can therefore be taken as a further indication that the niobium atoms are well dispersed in the silica matrix.

The Nb 3d signals of the pure niobia sample could be fitted with 2 Gaussians centered at 207.3 eV (FWHM = 1.5 eV) and 210.0 (FWHM = 1.5 eV), respectively. They area ratio is 2:3 as is typical for 3d levels in octahedral coordination [28]. Following the same approach as used for the oxygen signal, the Nb 3d spectrum of NS1 was deconvoluted by assuming that some niobium atoms should interact only with oxygens bonded to other niobium atoms. The signal was therefore deconvoluted into four peaks, two of them having the same binding energy and FWHM as found in pure niobia. The two new signals resulting from the deconvolution were centered at 207.9 eV (FWHM = 1.5 eV) and 210.6 eV (FWHM = 1.5 eV). The ratio between the areas of these two peaks was also about 3: 2. By comparing the areas of these peaks and the area of those assigned to pure niobium oxide it follows that about 85% of the niobium atoms in the NS1 sample have a different environment than the niobium atoms in the pure niobium oxide sample.

The Si 2p XPS shows two distinct signals in both silica and NS1. One symmetric peak is centered at 99.4 eV. This signal corresponds to the response of metallic silicon atoms of the support [36], which was exposed on some local spots. The Si^{4+} peak was centered at 103.8 eV (FWHM = 1.7 eV) in pure silica, and at 103.2 eV (FWHM = 1.9 eV) in the NS1 film. The shift of the silicon peak towards lower binding energies in the niobia–silica sample and its enlargement are further proof of a different atomic environment for silicon in the two materials.

4. Conclusions

The hydrogen and helium permeabilities of NS1 were one order of magnitude larger than NS2 and NS3. The H_2/CO_2 ideal separation factor was ~40 for NS1 and NS2 and 70 for NS3. These numbers indicate that NS1 is the most suitable sol of the three for the preparation of gas selective membranes. Because although the H_2/CO_2 selectivity was 60% higher in NS3 membranes than in NS1, the H_2 permeability of NS3 was 96% lower.

The results presented in this paper allowed us to establish a relationship between the gas transport properties of NS membranes and the structure of NS sols. The fabrication of microporous niobia–silica layers with thickness of a few tens of nanometers requires optimization of the synthetic conditions in order to obtain

sol particles with dimensions of a few nanometers. However a compromise must be reached, since insufficiently developed sols yield highly resistive microporous layers, as in the case of NS2.

XPS analysis on an NS1 film indicated that the sol–gel synthesis yielded a homogenous composite material with random distribution of Si and Nb. The surface of this mixed film interacted differently with CO_2 than pure silica and pure niobia surfaces do. The Nb loading in the composite should be chosen carefully, since the presence of Nb^{5+} ions in the silica network reduced the permeability of the material.

Acknowledgments

Financial support from the Netherlands Technology Foundation (STW) is gratefully acknowledged. The authors would like to thank the Netherlands Organization for Scientific Research (NWO) for giving us beam time to perform SAXS measurements at DUBBLE, and Dr. Kristina Kvashnina and Dr. Wim Bras (DUBBLE beam line) for on-site assistance at DUBBLE.

References

[1] V. Boffa, J.E. ten Elshof, A.V. Pethukov, D.H.A. Blank, Chem. Sus. Chem. 1 (2008) 437.
[2] J.-M. Jehng, I.E. Wachs, Catal. Today 8 (1990) 37.
[3] V. Boffa, D.H.A. Blank, J.E. ten Elshof, J. Membrane Sci. 319 (2008) 256.
[4] C.J. Brinker, G.W. Scherer, Sol–gel Science, Harcourt Brace Jovanovich, Boston, 1990.
[5] C.J. Brinker, T.L. Ward, R. Sehgal, N.K. Raman, S.L. Hietala, D.M. Smith, D.-W. Hua, T.J. Headley, J. Membrane Sci. 77 (1993) 165.
[6] J. Sekulic, J.E. ten Elshof, D.H.A. Blank, Adv. Mater. 16 (2004) 1546.
[7] A. Nijmeijer, H. Kruidhof, R. Bredesen, H. Verweij, J. Am. Ceram. Soc. 84 (2001) 136.
[8] A.J. Burggraaf, Fundamentals of Inorganic Membrane Science and Technology, Elsevier, Amsterdam, 1996.
[9] W. Bras, I.P. Dolbnya, D. Detollenaere, R. van Tol, M. Malfois, G.N. Greaves, A.J. Ryan, E. Heeley, J. Appl. Crystallography 36 (2003) 791.
[10] S.W. Provencher, Biophys. J. 16 (1976) 27.
[11] P.K. Maiti, T. Cagin, S.-T. Lin, W.A. Goddard, Macromolecules 38 (2005) 979.
[12] B.B. Mandelbrot, The Fractal Geometry of Nature, W.H. Freeman, New York, 1982.
[13] M.S. Dyuzheva, O.V. Kargu, V.V. Klyubin, Colloid J. 64 (2002) 33.
[14] R.J. Yong, P.A. Lovell, Introduction to Polymers, Chapman & Hall, London, 1991.
[15] P.J. Flory, J. Am. Chem. Soc. 58 (1936) 1877.
[16] P.J. Flory, J. Am. Chem. Soc. 63 (1941) 3091.
[17] E.B. Pereira, M.M. Pereira, Y.L. Lam, C.A.C. Perez, M. Schmal, Appl. Catal. A 197 (2000) 99.
[18] S.M. Maurer, D. Ng, El Ko, Catal. Today 16 (1993) 319.
[19] M. Suzana, P. Francisco, Y. Gushikem, J. Mater. Chem. 12 (2002) 2552.
[20] R.M. de Vos, H. Verweij, J. Membrane Sci. 143 (1998) 37.
[21] R.R. Bhave, Inorganic Membranes: Synthesis, Characteristics and Applications, Van Nostrand Reinhold, New York, 1991.
[22] V. Boffa, J.E. ten Elshof, D.H.A. Blank, Micropor. Mesopor. Mater. 100 (2007) 173.
[23] J.H. Jehng, I.E. Wachs, Catal. Today 8 (1990) 37.
[24] R.K. Iler, The Chemistry of Silica: Solubility, Polymerization, Colloid and Surface Properties, and Biochemistry, John Wiley and Sons, New York, 1979.
[25] R.S.A. de Lange, K. Keizer, A.J. Burggraaf, J. Membrane Sci. 104 (1995) 81.
[26] B.N. Nair, K. Keizer, H. Suematsu, Y. Suma, N. Kaneko, S. Ono, T. Okubo, S.-I. Nakao, Langmuir 16 (2000) 4558.
[27] R.J.R. Uhlhorn, K. Keizer, A.J. Burggraaf, J. Membrane Sci. 66 (1992) 271.
[28] M. Kanezashi, T. Fujita, M. Asaeda, Sep. Sci. Technol. 40 (2005) 225.
[29] T. Yoshioka, E. Nakanishi, T. Tsuru, M. Asaeda, AIChE J. 47 (2001) 2052.
[30] K. Yoshida, Y. Hirano, H. Fujii, T. Tsuru, M. Asaeda, J. Chem. Eng. Jap. 34 (2001) 523.
[31] M. Cerruti, C.L. Bianchi, F. Bonino, A. Damin, A. Perardi, C. Morterra, J. Phys. Chem. B 109 (2005) 14496.
[32] M. Cerruti, C. Morterra, Langmuir 20 (2004) 6382.
[33] J.J. Senkevich, G.-R. Yang, T.-M. Lu, D.W. Sherrer, Appl. Phys. A 77 (2003) 581.
[34] M.K. Bahl, J. Phys. Chem. Solids 36 (1975) 485.
[35] L.C.A. Oliveira, T.C. Ramalho, M. Goncalves, F. Cereda, K.T. Carvalho, M.C. Nazzarro, K. Sapag, Chem. Phys. Lett. 446 (2007) 133.
[36] C.D. Wagner, J. Vac. Sci. Technol. 15 (1978) 518.